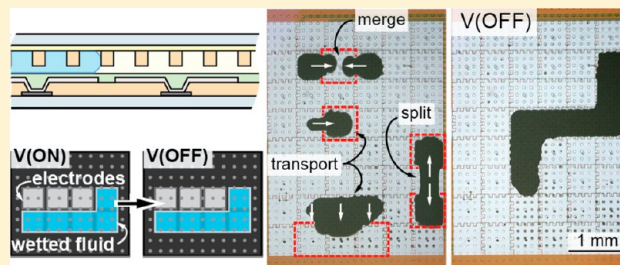


Investigation of Laplace Barriers for Arrayed Electrowetting Lab-on-a-Chip

A. Schultz, I. Papautsky, and J. Heikenfeld*

Department of Electrical Engineering and Computing Systems, University of Cincinnati, Cincinnati, Ohio 45221, United States

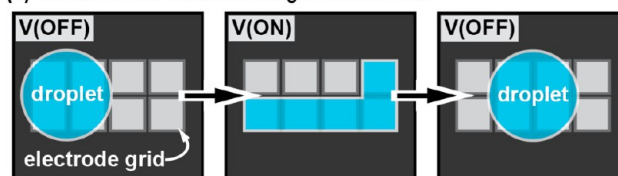
ABSTRACT: Partial-post Laplace barriers have been postulated as a means to allow electrowetting transport and geometrical reshaping of fluids, followed by the preservation of fluid geometry after the electrowetting voltage is removed. Reported here is the first investigation of Laplace barriers with the arrayed electrodes and splitting/merging transport functions for an electrowetting lab-on-a-chip. Laplace barriers optimized for $500 \times 500 \mu\text{m}^2$ electrodes and $78 \mu\text{m}$ channel height are shown to provide geometrical control of fluid shape down to radii of curvature of $\sim 70 \mu\text{m}$. The Laplace barriers increase the splitting volume error, but with proper electrical control, the average error in the split volume is reduced to 5%. Improved programmable fluid storage in droplets or reservoirs and continuous channel flow are also shown. This work confirms the potential benefits of Laplace barriers for lab-on-a-chip and also reveals the unique challenges and operation requirements for Laplace barriers in lab-on-a-chip applications.



INTRODUCTION

Microfluidics is the driving force behind lab-on-a-chip (LOC) devices that have been developed for medical diagnostics,^{1–6} chemical^{1,7–9} and biological sensing,^{1,4,10–13} and environmental monitoring.^{12–14} These devices primarily use one of two distinct methods to handle micro/nanoscale volumes of fluids: (1) fixed-channel continuous flow or two-phase microfluidics¹⁵ or (2) discrete droplet-based microfluidics. Where continuous flow devices certainly have advantages with respect to simplicity, reliability, manufacturability, and throughput,¹⁶ the discretization of microfluidics, also known as digital microfluidics (DMF), can have advantages in programmability, simplified experiment redesign, reusability, and parallel processing.^{16–18} Recently, researchers have begun to unify the advantages of continuous channel microfluidics and DMF by (1) directly integrating fixed, continuous flow channels with a small electrowetting DMF grid array;^{19,20} (2) creating reconfigurable virtual electrowetting channels;^{21,22} or (3) integrating Laplace barriers to maintain electrically programmed geometries even when the voltage is removed^{23,24} (Figure 1). The value of Laplace barriers for LOC has been speculated upon in prior reports but has not yet been demonstrated nor the true challenges and requirements understood. Reported here is the first investigation of Laplace barriers with the arrayed electrodes and splitting/merging transport functions for electrowetting LOC. This investigation includes a demonstration of electrowetting channel segment formation and preservation without voltage, theory, and experiment with respect to the important functions of droplet merging and splitting, improved fluid storage, and a demonstration of continuous channel flow. This work confirms the potential benefits of Laplace barriers for fluid stability and control for reservoirs, droplets, and channels and also reveals

(a) conventional electrowetting microchannel



(b) electrowetting with grid of Laplace barriers

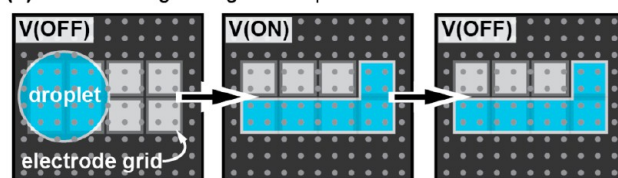


Figure 1. Simple top-view diagrams of the functional difference between electrowetting a channel segment (a) without or (b) with Laplace barriers.

the unique challenges and operation requirements for Laplace barriers in LOC applications where both digital droplet control with zero voltage stability and fluid flows are desired on a single platform.

FABRICATION AND EXPERIMENT

Figure 2 shows the cross-sectional view of the fabricated test devices. Each device consists of a two-plate design with a bottom electrowetting electrode array plate and a top plate with a grounding

Received: January 23, 2014

Revised: April 14, 2014

Published: April 16, 2014

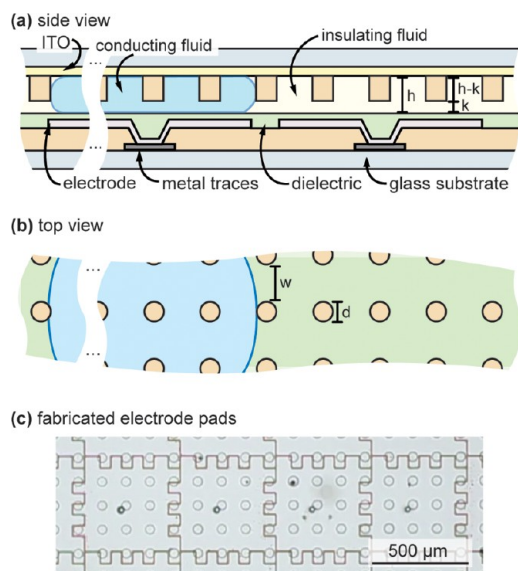


Figure 2. Cross-section of the fabricated device: (a) side view, (b) top view, and (c) top view photograph. All internal surfaces of the device are coated with a thin hydrophobic fluoropolymer (not shown in (a) or (b)).

electrode and an array of partial-post²³ Laplace barriers. The bottom electrode array was 6×8 (48 total electrodes), each with a $500 \times 500 \mu\text{m}^2$ area. To allow individual electrical control of each electrode, the following film stack was utilized: a bottom metal trace layer, a via layer to connect to a top metal electrowetting pad layer, and all electrowetting pads covered by a hydrophobic dielectric layer to enable the electrowetting effect.²⁵

The bottom plate (electrowetting array) fabrication began with solvent cleaning of $50.8 \times 50.8 \text{ mm}^2$ and 1.1-mm-thick Corning 1737 boro-aluminosilicate glass substrates. For the bottom electrowetting plate, the glass was deposited with 150 nm of nickel by thermal evaporation. The nickel was photolithographically patterned and wet etched into $300\text{-}\mu\text{m}$ -wide traces for connection to an external computer-controlled electrical driver board (not shown). Onto the patterned nickel, Fujifilm AP2210B photodefinable polyimide was spin-coated to a $5 \mu\text{m}$ thickness, photolithographically patterned, developed, and hard-baked with $15\text{-}\mu\text{m}$ -diameter via holes to the bottom metal layer. Aluminum (100 nm) was then sputtered deposited, photolithographically patterned with a Microposit Shipley S1800 series photoresist, and etched into a grid array of interdigitated electrowetting pads with a $500 \mu\text{m}$ pitch. The bottom plate was then conformally coated with an $\sim 400 \text{ nm}$ Parylene HT dielectric ($\epsilon_r \approx 2.2$, Specialty Coating Systems). This dielectric was then made hydrophobic by coating with a monolayer of Cytonix Fluoropel 1601 V fluoropolymer using a surface grafting process described by Berry et al.,²⁶ including a final hard bake for 30 min at 180°C which reduces the surface energy to $\sim 16 \text{ mN/m}$.

The top plate (grounding electrode, Laplace barriers) fabrication began with the same glass used for the bottom plate, but the glass also included an $\text{In}_2\text{O}_3/\text{SnO}_2$ (ITO) transparent electrode. To create the Laplace barriers, a PerMX 3050 ($50 \mu\text{m}$) dry film photoresist was laminated and photolithographically patterned into an array of circular posts (Laplace barriers) and part of the channel height spacing layer around the perimeter of the substrate. To complete the channel height, two additional layers of PerMX 3014 ($28 \mu\text{m}$ total) were then sequentially laminated on top of the previous spacer layer, photolithographically patterned outside the perimeter of the post array, and hard baked to support a total channel height of $78 \mu\text{m}$. The top plate was then made hydrophobic using the same process used for the bottom plate to achieve a hydrophobic monolayer, sufficiently thin that the ITO electrode is not electrically insulated from the conducting fluid.

The electrowetting fluid system used in testing consisted of a custom pigment dispersion from Sun Chemical as the electrically conducting fluid and an isoparaffin oil as the insulating fluid. This particular pigment dispersion was chosen simply because it is easy to visualize, it is nonaqueous, which increases the device reliability,²⁷ and it can be used as a surrogate for biofluids²⁸ as long as suitable measures are taken to prevent fouling and absorption.²⁹ This fluid system has an interfacial surface tension of 10 mN/m , and previously we presented a theory that proves that higher-surface-tension fluids such as pure water are equally viable.^{23,24} A simple “smash-dosing” method was used to dose the device where a drop of insulating fluid was first placed on the electrode grid with a pipet and a smaller drop of conducting fluid was dispensed by micropipet near an electrode within the droplet of insulating fluid. The top partial-post plate was placed on top of the bottom plate and aligned so that the posts were straight along the edges of the electrowetting electrode pads. The bottom and top plates were then clamped together. Any remainder of the channel that was not fully filled with insulating fluid was filled by simple edge dosing (capillarity between the top and bottom plates). This technique was used to prove the concept and is not necessarily representative of LOC applications. Proper LOC fluid handling capabilities will be integrated in the future.

■ LAPLACE BARRIER DESIGN

When a voltage is applied to an electrowetting electrode, an electromechanical force attracts the conducting fluid to that electrode. A detailed review of this mechanism can be found elsewhere.²⁵ A brief review of the theoretical behavior of Laplace barriers^{23,24} is now provided. With the integration of partial-post Laplace barriers into an electrowetting system (Figure 1b), voltage is used to reshape or transport the conducting fluid, and when the voltage is removed, the fluid retains the shape that it was electrowetted to because the radii of curvatures between and under the Laplace barriers impart a Laplace pressure which prevents the droplet from returning to a circular shape in the channel. With the assumption that the electrowetted contact angle (θ_B) is 90° and the top plate contact angle (θ_T) is 180° , and the mechanics governing the threshold for fluid transport using Laplace barriers simplify to the following equations

$$\Delta p_b^{\text{tr}} = \gamma_{ci} \left(\frac{1}{h} + \frac{2}{w} \right) \quad (1)$$

$$\Delta p_u^{\text{tr}} = \gamma_{ci} \left(\frac{-2}{d} - \frac{1}{k} \right) \quad (2)$$

$$\Delta p_R = \gamma_{ci} \left(\frac{2}{h} \right) \quad (3)$$

where eqs 1 and 2 are threshold Laplace pressures on the advancing (electrowetted) end of a droplet to depin the conducting fluid from between and under the posts, respectively, and eq 3 is the driving pressure from the receding end of the droplet. The interfacial surface tension between the conducting and insulating fluids is γ_{ci} , the channel height is h , the width between the posts is w , the diameter of the posts is d , and the height under the posts is k . For fluid transport to occur, electrowetting must reduce the pressure on the advancing edge of the droplet such that Δp_R exceeds either Δp_u^{tr} or Δp_b^{tr} . Importantly, Δp_u^{tr} or Δp_b^{tr} is carefully designed for the maximum channel open area, and these are nearly equal such that neither mode of transport (between or under) dominates because purely under transport is slower (smaller effective channel height) and purely between transport causes the droplet to break up into capillary fingers.^{23,24} In this work, the parameters

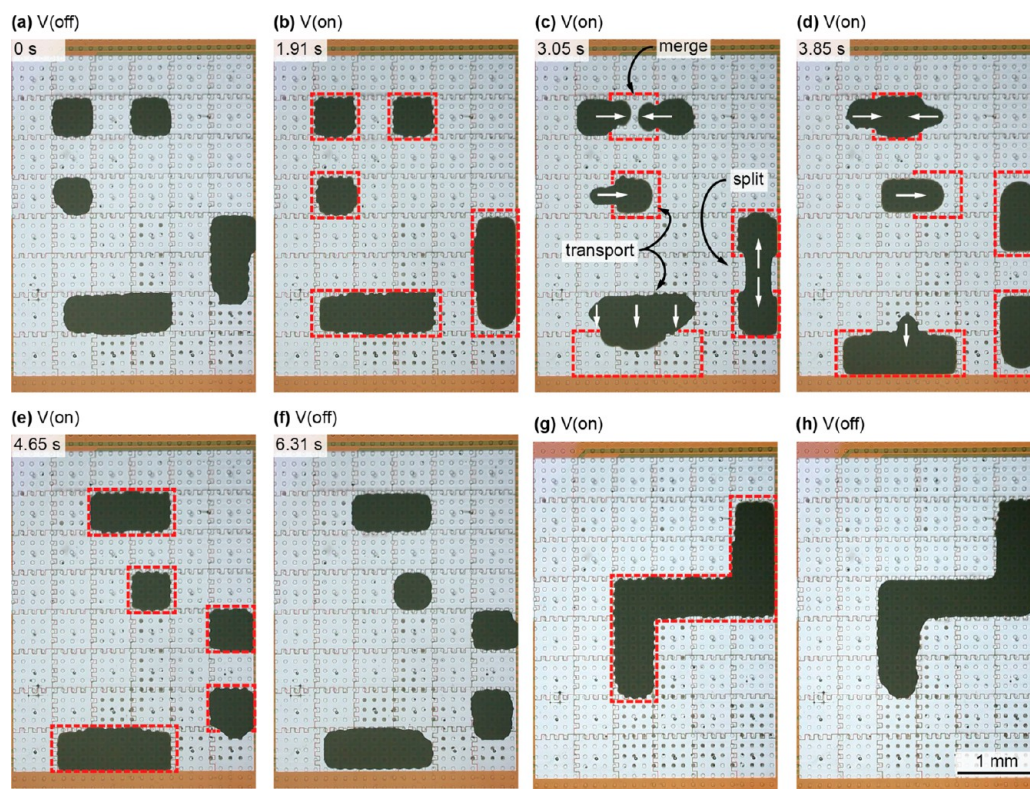


Figure 3. Photographs of (a–e) fluid storage, transport, merging, splitting, and again storage. Photographs (f–g) show geometrically stable fluid segments. The dashed red boxes around electrodes indicate electrowetting (voltage). Each electrode is 500 μm wide.

satisfying the above design criteria were found to be $h = 78 \mu\text{m}$, $d = 50 \mu\text{m}$, $k = 28 \mu\text{m}$, and $w = 75 \mu\text{m}$. With these dimensions, a minimum required “threshold” voltage of $\sim 45 V_{\text{pp}}$ was needed for transport to or draw a droplet from a reservoir.

■ DEMONSTRATION OF BASIC DMF OPERATIONS

The basic DMF operations for the LOC functionality (transport, splitting, and merging) have been demonstrated and characterized in this study using an applied voltage of 75 V_{pp} , 120 Hz square-wave supplied by a custom, computer-controlled driver board. Photographs of a simultaneous demonstration of all basic operations are shown in Figure 3. Figure 3a shows the tested device with the electrical voltage turned off on all electrodes to demonstrate the concept of controlled fluid confinement to noncircular shapes. In Figure 3b, the voltage is applied only where the black conducting fluid is. Figure 3c,d demonstrates all basic DMF operations occurring simultaneously (merging, transporting, and splitting) where the drawn dashed red boxes indicate where voltage is applied. As shown, transporting was demonstrated with both a discrete droplet and a larger multielectrode volume of fluid. Figure 3e demonstrated the final locations of all droplets/segments immediately after completion of the fluid movements with the electrical voltage still applied, and Figure 3f is the same except with the voltage off. The images shown in Figure 3f clearly show the ability to retain noncircular fluid geometries. The performance of confinement can be measured by the radii of curvature (r) at the corners of fluids and between individual Laplace barrier posts, which in this work averages $r \approx 70 \mu\text{m}$. Figure 3g,h also shows a longer “channel” segment of fluid formed at a later time with the same droplets, with both the voltage on and off. Distinct from some of our previous

work^{21,22} in creating virtual electrowetting channels, these channel segments are stable even as the voltage is removed. With the integration of continuous flow inlets and outlets into this system, a zero voltage fluid channel stability can be realized when fluid flows are stopped, allowing for further fluid manipulation to be performed and fluid flows to be resumed with the same or a reconfigured fluid channel.²¹ Some staining of the post tops is notable in Figure 3 and will be seen in Figure 5 also. This staining is an artifact of the stability of the custom pigment dispersion utilized (is not seen with most other fluids) and is not well understood at this time but is also attributed to fabrication. The posts were fabricated with sharp, squared-off corners that can lead to weak spots in the fluoropolymer. This can be overcome by fabricating posts with rounded tops or by taking greater care during the assembly of the device.

■ FLUID TRANSPORT VELOCITIES

The dynamics of a droplet transported from one electrode to another using a traditional DMF system have been reported by other groups in detail.^{30–32} Where the trends found in those studies are similar to a system utilizing Laplace barriers with regard to scaling, fluid systems, and applied voltages, the instantaneous displacement and velocity profiles deviate significantly and are shown in Figure 4. Fluid displacement with respect to leading and trailing end initial locations is shown in Figure 4a. The deviation from leading and trailing end displacements lead to velocity peaks at different instances and a more constant droplet center velocity profile (Figure 4b) during droplet transport. As demonstrated by Pollack et al.,³⁰ traditional DMF systems differ significantly from this observation and experience similar leading and trailing end displacements during transport; therefore, droplet center

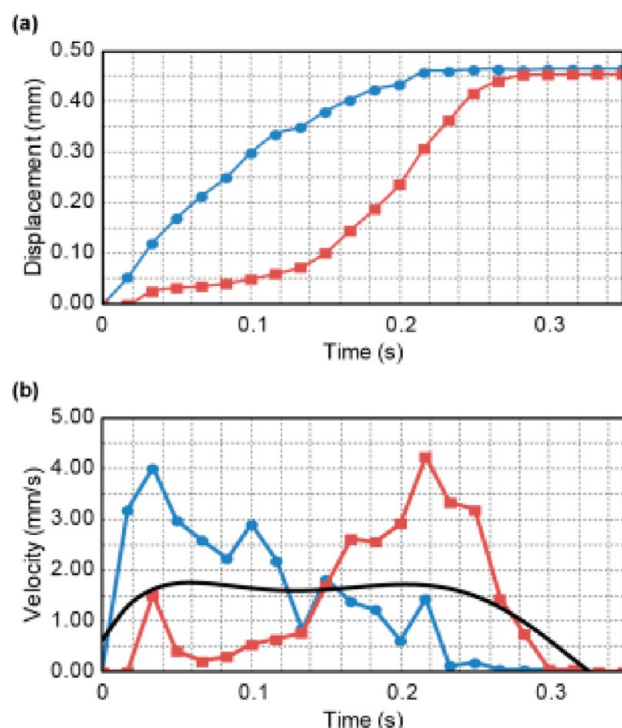


Figure 4. Image analysis measurements of droplet (a) displacement from the initial location and (b) instantaneous velocities as functions of time during single droplet transport to an adjacent electrode. The blue lines with circular markers and red lines with square markers are leading and trailing end measurements, respectively. The black line is a fifth-order polynomial fit of the droplet center velocities based on differentiation from the displacement measurements.

velocities increase to a peak velocity and then decay at a similar rate until the droplet transport is complete. This deviation from traditional DMF systems is due to fluid pinning on the posts of the trailing end of the droplet. With an applied voltage of 75 V_{pp} , 120 Hz square-wave, the average transport velocities ranged from 2 to 3 mm/s with transfer rates from 4 to 6 Hz. By reducing the voltage to 45 V_{pp} , we reduced the transfer rates to ~ 1.6 Hz. Increasing the voltage did not significantly increase transport velocities due to electrowetted contact angle saturation. As demonstrated in our previous work, by utilizing a higher interfacial tension fluid system and following the suggestions therein, these transport velocities and transfer rates will increase.

DETAILED STUDY OF SPLITTING ACCURACY

Fluid splitting in DMF systems occurs with droplet elongation in two opposite directions with a nonenergized electrode in the center causing a pinching effect in the middle. According to Cho et al.,³³ splitting in a traditional DMF system, neglecting contact angle hysteresis, can be represented in terms of the channel height, the advancing and necking radii of curvature, R_2 and R_1 , respectively, and the top and bottom contact angles with the following equation:

$$\frac{R_2}{R_1} = 1 - \frac{R_2}{h}(\cos \theta_B - \cos \theta_T) \quad (4)$$

When we make the same assumptions for splitting as for fluid transport, eq 4 becomes

$$\frac{R_2}{R_1} = 1 - \frac{R_2}{h} \quad (5)$$

where reducing the channel height or increasing the advancing horizontal radius with electrode size or both will improve the splitting performance. This basic equation can also be used for DMF systems with integrated partial-post Laplace barriers as a general guideline; however, there are significant differences in the mechanics of the pinching effect that are not seen with traditional DMF systems.

Figure 5 shows sequenced photographs of a typical droplet split when using partial-post Laplace barriers. The radii of

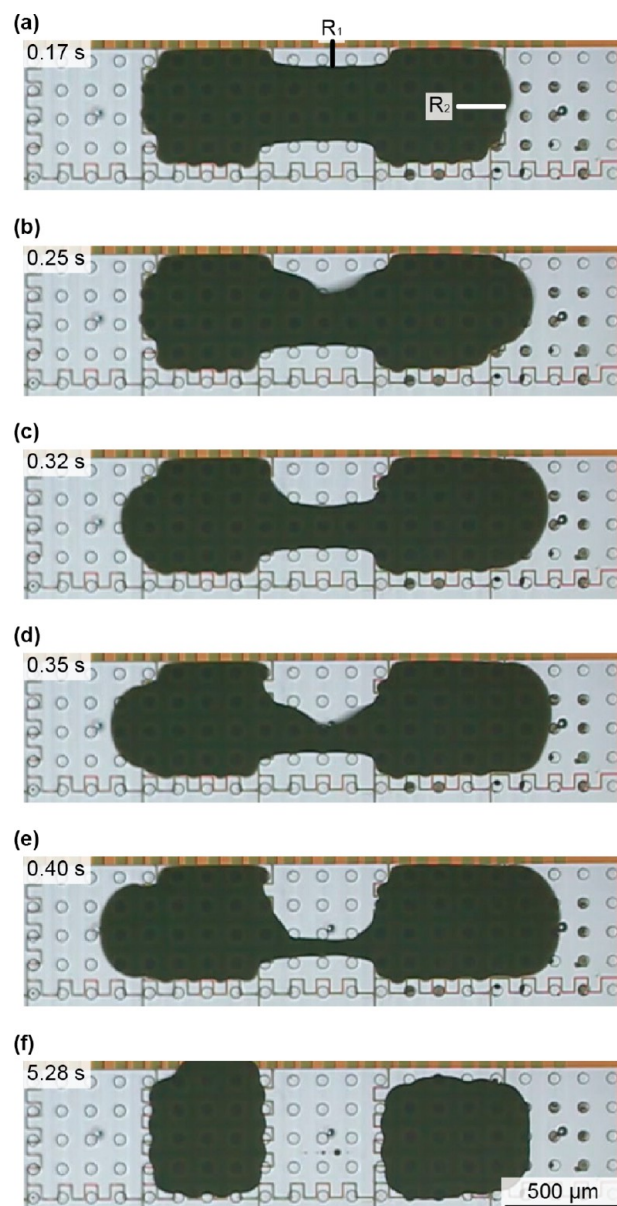


Figure 5. Sequenced photographs of droplet splitting. Scale: each electrode is 500 μm wide.

curvatures are clearly impacted by the Laplace barriers. As shown in Figure 5a, when necking began and the fluid pinched over the center electrode, the fluid was pinned to the inside edges of the first rows (top and bottom) of the Laplace barriers. This imparts a fluid geometry consisting of a series of larger

negative radii of curvature between each post. As the fluid continued to elongate longitudinally (Figure 5b), the fluid first depinned from the center post, creating a smaller necking radius of curvature between the first and second rows of posts, longitudinally depinning from adjacent posts in both directions until the fluid pinned to the inside edges of the next row of posts. As the fluid continued to elongate, the pin–depin–shift effect occurred with each row of posts (Figure 5c–e) until the droplet finally split into two discrete droplets and the voltage was removed (Figure 5f). This behavior suggests that the number of posts is odd across each electrowetting pad such that the depinning is centered midway to promote equal splitting volumes.

This sequence of fluid pinning to and depinning from the posts does not necessarily change the overall predictability of fluid splitting in the system when using eq 4 or 5, but as noted, post diameter, alignment/location, post height, and the space between posts are extra factors that can affect how the fluid splits.

■ MAXIMIZING SPLITTING ACCURACY

Splitting techniques for traditional DMF systems range from the most simplified³³ to several more complex improvements that incorporate a variety of integrated sensing tools including impedance measurements,^{11,34–36} optical detection,^{37–39} high-resolution multielectrode control,¹¹ and voltage ramping.^{21,40} However, due to the integrated Laplace barriers and no presence of sensing tools other than peering through a microscope, the only way to improve splitting accuracy in this work is through fluid shifting and software timing.

Plots of splitting accuracy over several splits as well as sequenced photographs are shown in Figure 6a,b using two different splitting routines. Areas and perimeters of each droplet (no voltage) were determined using image processing (ImageJ), and then volumes were calculated by compensating for the posts within the fluid areas as well as fluid geometries (rounded edges instead of straight) based on the fluid system used. The first “basic” routine, based on the splitting routine discussed by Cho et al.,³³ started with fluid confined to two horizontally adjacent electrodes, and then a voltage was applied to one of the two electrodes. The two horizontally adjacent electrodes from this center electrode were then turned on while the intermediate electrode was simultaneously turned off, forcing the fluid to split into two disproportionate droplets as indicated in Figure 6a and demonstrated in the corresponding sequenced photographs. The fluid was then remerged and returned to its original location.

Despite the disproportionality of the droplet volumes, the droplets did split with relative repeatability. The top droplet consistently split into the same volume for each split, as did the bottom. The difference in volume was a result of the integration of the Laplace barriers and the inability to center the fluid over one electrode. The inability to achieve this centering occurs because the Laplace pressure on the advancing end is too large for the receding end to drive the entire droplet to shift enough to center over one electrode. In contrast, the droplets in traditional DMF systems are already centered over a single electrode, allowing for semiequal splitting between the two adjacent electrodes. Therefore, this method by Cho et al. is incompatible with a DMF system using Laplace barriers if equal split volumes are required.

Figure 6b shows the results using a more advanced splitting routine that centers the fluid on one electrode and then splits it

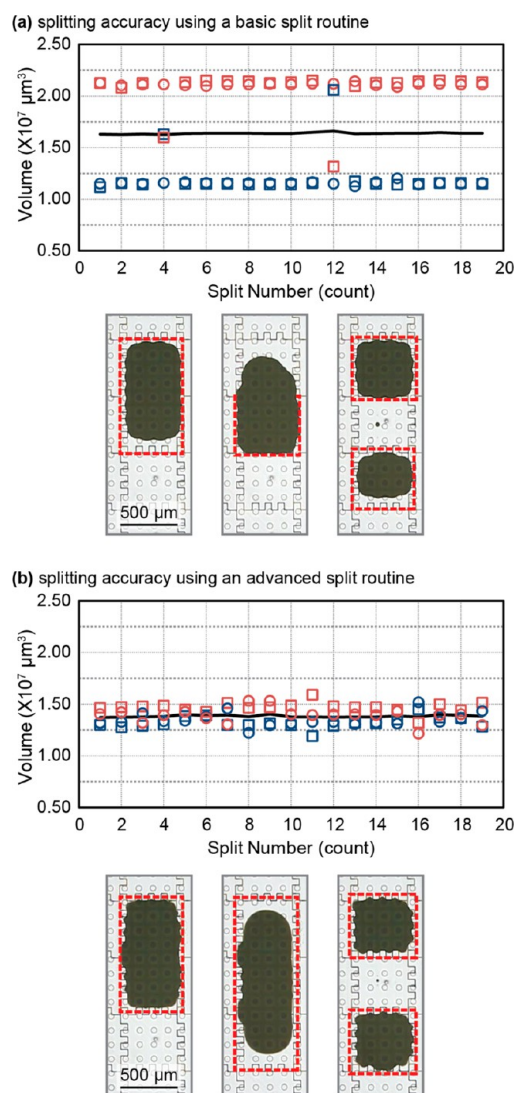


Figure 6. Plots of splitting accuracy and photographs using (a) a basic (traditional) splitting routine and (b) an advanced splitting routine, which is necessary when using Laplace barriers. Each data point color, red or blue, represent the top or bottom split droplets, respectively, and the shapes, circle or square, represent a 500 or 2000 ms split dwell time. The dashed red boxes in the photographic sequences indicate an applied voltage.

into two evenly sized droplets. This routine used the same confined droplet as the previous routine, except that the two electrodes remained with the voltage on and a third adjacent electrode was turned on, forcing the droplet to stretch slightly across the three electrodes. A timed shift of the fluid, by pulsing the voltage of the receding electrode off and then back on, allowed for the droplet to be shifted and centered over the intermediate electrode. The routine continued with the voltage being removed from the intermediate electrode and then the larger droplet splitting into two equally sized droplets. By using this method, the splitting accuracy was much improved and either droplet averaged an ~5% variation from the nominal volume. This is also consistent with other methods that we have previously reported, where adjusting the time allowed for the droplet to dwell in the necking state³³ improves the splitting accuracy. With Laplace barriers, a shorter dwell time of 500 ms yielded an ~6.0% average splitting error whereas a

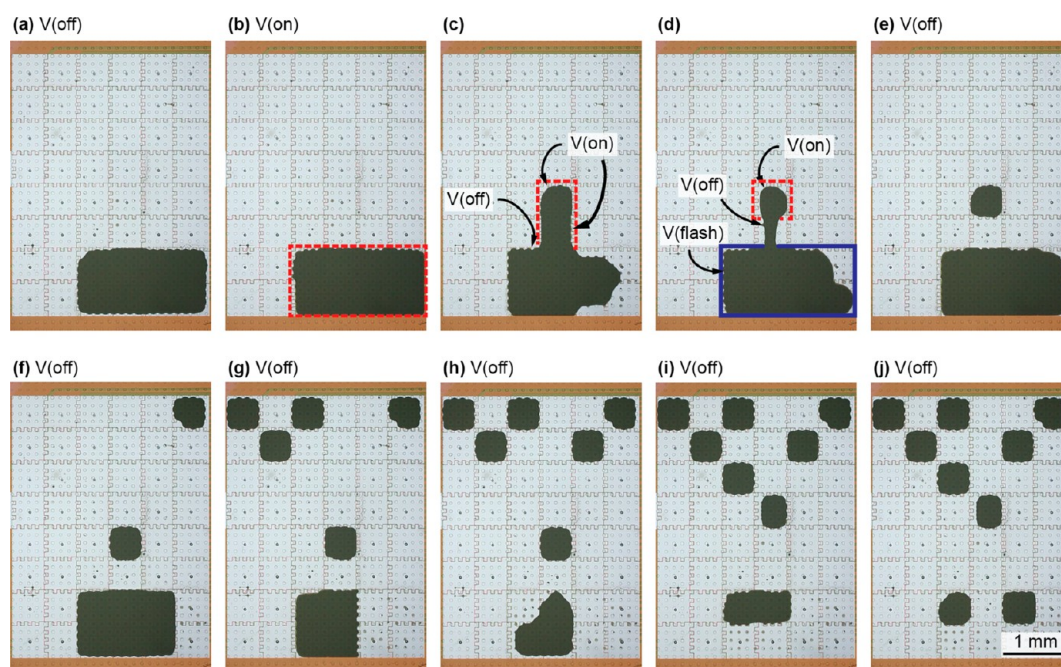


Figure 7. (a–e) Demonstration of fluid storage with no applied voltage and sequenced photographs of dispensing a droplet from a larger storage area or reservoir. (f–j) Continuation of dispensing from the reservoir one droplet at a time and transporting to a specified location until the depletion of the reservoir. Each photograph was taken when there was no applied voltage.

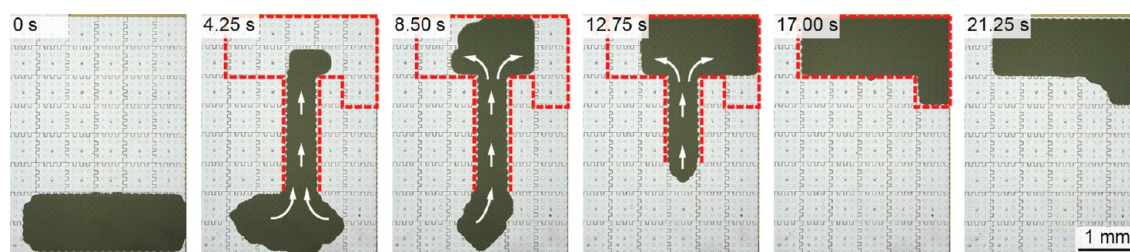


Figure 8. Generating fluid flows with continuous flow control where voltages are held constant on the advancing channel and reservoir and then completely removed.

longer dwell time of 2 s yielded an improved $\sim 4\%$ average error.

On the basis of these results, by integrating Laplace barriers into a DMF system and incorporating a more improved splitting technique, splitting accuracies comparable to those of traditional DMF systems can be achieved.^{36,41,42} Further improvement is possible with this splitting technique if an automated imaging feedback or impedance setup is used to sense how far the fluid has shifted and to adjust the shift time automatically or compensate for an under or over shift of fluid.

FLUID STORAGE AND STABILITY

Another advantage of using Laplace barriers for electrowetting-based DMF is increased control for fluid storage. Not only can fluids be packed adjacent to one another with greater reliability and less risk of unintended merging, but large volumes (reservoirs) of fluid can be electrically configured on demand into more complex shapes. Figure 7 demonstrates this concept where a large virtual reservoir was formed, from which discrete droplets can be pulled, transported, and stored in a tight packing fashion (immediately adjacent corners). As shown in Figure 7a, a large virtual fluid reservoir was formed over eight electrodes, the voltage was removed from the device, and the reservoir remained tightly confined. Figure 7b–e demonstrates

the process of dispensing fluid from this virtual reservoir. With Laplace barriers, the reservoir can have the voltage removed from it while the fluid is pulled with adjacent electrodes, and the reservoir still holds its primary shape. This is demonstrated in Figure 7c. However, as shown in Figure 7d, in order to fully split a discrete droplet from the bulk, it was determined that the fluid must be pulled at least two electrodes away from the bulk to form a small channel, the voltage must be removed from the intermediate electrode between the end of the channel and the bulk of the reservoir, and then the voltage on the remaining fluid in the reservoir must be briefly pulsed to rewet the remaining fluid to a new geometry for the reduced-volume reservoir. As more fluid is removed from the reservoir, the volume is reduced and the shape and number of electrodes that are pulsed during the dispensing process must be changed as well. This also leads to more complex reservoir configurations that can be reconfigured during a process to utilize the number of available electrodes more efficiently, even with the voltage removed. It is worthwhile to highlight that the adjacent-corner packing achieved for droplets in the stored state and the complex reservoir configurations have no risk of shifting or merging even if the setup is exposed to the effects of gravity, vibration, or nonlevel orientations.

■ GENERATING FLUID FLOWS

Continuous flows of fluid in a virtual channel add functionality beyond that of traditional DMF, including the use of larger reagent and sample sizes for greater throughput with reduced energy consumption. Virtual channel formation based on the work of Banerjee et al.²¹ is demonstrated in Figure 3 with the added capability here of retaining the channel geometry even without an applied voltage. With this, the generation of fluid flows can be realized, as demonstrated in Figure 8 where fluid was transported from one large reservoir through a virtual channel to form another large reservoir with a continuous flow control method where voltages are constantly applied to the advancing channel and reservoir. As the fluid enters the virtual channel, the trailing electrodes are turned off to continue the flow until the new reservoir is formed.

The primary benefits of this control method apply to reagents and washes that require larger volumes of fluids compared to fluid samples. By eliminating the need to split and move droplets one at a time from a reservoir, this control method can increase throughput while simultaneously reducing the control logic and timing necessary for discrete droplet transport. The flow rate can also be adjusted by altering the amplitude of the activated electrodes. Furthermore, once the channel is formed, the voltage can be removed and the channel will remain in its shape, as discussed previously, to reduce energy consumption and to allow on/off control of the flow.

■ FURTHER DISCUSSION AND CONCLUSIONS

With the basic operations demonstrated in this work, DMF with Laplace barriers is shown to have the potential to perform the traditional range of DMF applications, such as DNA analysis,^{6,43} chemical reactions,^{7,9} immunoassays,^{5,44,45} proteomics,⁴⁶ and cell-based assays.⁴⁷ Despite the initial validation that this work provides, there are inherent drawbacks for Laplace barriers such as slightly reduced transport speeds,^{23,24} fluid pinning, and some reduction in splitting accuracies. Where transport speeds and fluid pinning are the lesser of the drawbacks, the splitting accuracy is likely the most important challenge to overcome. We postulate that the advantages of Laplace barriers can be retained and the splitting accuracy can be greatly improved using electrical/optical feedback or finer-pitch electrode control. Finer-pitch electrical control using an active matrix array of thin film transistors on glass^{11,48} is readily available commercially, as it is the technology used to drive the fine-pitch pixels in all high-performance liquid-crystal displays. The Laplace barrier pitch would remain the same, but the electrode pitch could be reduced to 1, 2 × 2, 3 × 3 and so forth electrodes between each Laplace barrier unit cell (as defined by the Laplace barrier posts). These electrodes could be switched on and off to improve the resolution of control for all DMF functions.

There is one further hybrid solution to maintain the advantages of Laplace barriers while resolving the disadvantages. Even if the splitting accuracy is not up to the same standards as traditional DMF systems, partial-post Laplace barriers can be integrated such that they cover only a certain portion of the electrode grid to allow regions of the DMF system to provide traditional splitting.^{33,36,41,42} This is easily achieved, as Laplace barriers are formed on the top plate, and simply would not be included in certain areas of the LOC device. Furthermore, components of the continuous flow of

fluid could be integrated into this system,²¹ and other forms of continuous channel functionality would be possible.

In conclusion, this work demonstrates the basic LOC functionalities and related advantages provided by Laplace barriers including improved droplet or reservoir storage and channel/segment/droplet stability with zero applied voltage. Furthermore, with the ability to generate fluid flows with the larger fluid volumes needed for reagents and washes, an increase in throughput with more simplified electrical control is possible. Techniques are provided to improve performance, specifically in achieving repeatable fluid splitting. Furthermore, several methods are postulated which could resolve any remaining deficiencies with respect to utility for LOC applications.

■ AUTHOR INFORMATION

Corresponding Author

*E-mail heikenjc@ucmail.uc.edu; phone: +1 (513)556-4763.

Notes

The authors declare no competing financial interest.

■ ACKNOWLEDGMENTS

We gratefully acknowledge partial support from NSF IHCS award no. 1001141, funding from the state of Ohio for the creation of the Ohio Center for Microfluidic Innovation, and advanced materials provided by Specialty Coating Systems, Inc. (Parylene HT) and Sun Chemical (fluid systems).

■ REFERENCES

- (1) Jebra, M. J.; Bartsch, M. S.; Patel, K. D. Digital microfluidics: a versatile tool for applications in chemistry, biology and medicine. *Lab Chip* **2012**, *12*, 2452–2463.
- (2) Mao, X.; Huang, T. J. Microfluidic diagnostics for the developing world. *Lab Chip* **2012**, *12*, 1412–1416.
- (3) Paul, Y.; Thayne, E.; Elain, F.; Kristen, H.; Kjell, N.; Milton, R. T.; Bernhard, H. W. Microfluidic diagnostic technologies for global public health. *Nature* **2006**, *442*, 412–418.
- (4) Rivet, C.; Lee, H.; Hirsch, A.; Hamilton, S.; Lu, H. Microfluidics for medical diagnostics and biosensors. *Chem. Eng. Sci.* **2011**, *66*, 1490–1507.
- (5) Sista, R. S.; Eckhardt, A. E.; Wang, T.; Graham, C.; Rouse, J. L.; Norton, S. M.; Srinivasan, V.; Pollack, M. G.; Tolun, A. A.; Bali, D.; Millington, D. S.; Pamula, V. K. Digital Microfluidic Platform for Multiplexing Enzyme Assays: Implications for Lysosomal Storage Disease Screening in Newborns. *Clin. Chem.* **2011**, *57*, 1444–1451.
- (6) Schell, W. A.; Benton, J. L.; Smith, P. B.; Poore, M.; Rouse, J. L.; Boles, D. J.; Johnson, M. D.; Alexander, B. D.; Pamula, V. K.; Eckhardt, A. E.; Pollack, M. G.; Benjamin, D. K.; Perfect, J. R.; Mitchell, T. G. Evaluation of a digital microfluidic real-time PCR platform to detect DNA of *Candida albicans* in blood. *Eur. J. Clin. Microbiol. Infect. Dis.* **2012**, *31*, 2237–2245.
- (7) Boles, D. J.; Benton, J. L.; Siew, G. J.; Levy, M. H.; Thwar, P. K.; Sandahl, M. A.; Rouse, J. L.; Perkins, L. C.; Sudarsan, A. P.; Jalili, R.; Pamula, V. K.; Srinivasan, V.; Fair, R. B.; Griffin, P. B.; Eckhardt, A. E.; Pollack, M. G. Droplet-Based Pyrosequencing Using Digital Microfluidics. *Anal. Chem.* **2011**, *83*, 8439–8447.
- (8) Keng, P. Y.; Chen, S.; Ding, H.; Sadeghi, S.; Shah, G. J.; Dooraghi, A.; Phelps, M. E.; Satyamurthy, N.; Chatzioannou, A. F.; Kim, C.-J. C.; van Dam, R. M. Micro-chemical synthesis of molecular probes on an electronic microfluidic device. *Proc. Natl. Acad. Sci. U.S.A.* **2012**, *109*, 690–695.
- (9) Karuwan, C.; Sukthang, K.; Wisitorsa, A.; Phokharatkul, D.; Patthanasettakul, V.; Wechsathol, W.; Tuantranont, A. Electrochemical detection on electrowetting-on-dielectric digital microfluidic chip. *Talanta* **2011**, *84*, 1384–1389.

- (10) Scullion, M. G.; Di Falco, A.; Krauss, T. F. Slotted photonic crystal cavities with integrated microfluidics for biosensing applications. *Biosens. Bioelectron.* **2011**, *27*, 101–105.
- (11) Hadwen, B.; Broder, G. R.; Morganti, D.; Jacobs, A.; Brown, C.; Hector, J. R.; Kubota, Y.; Morgan, H. Programmable large area digital microfluidic array with integrated droplet sensing for bioassays. *Lab Chip* **2012**, *12*, 3305–3313.
- (12) Delattre, C.; Allier, C. P.; Fouillet, Y.; Jary, D.; Bottausci, F.; Bouvier, D.; Delapierre, G.; Quinaud, M.; Rival, A.; Davoust, L.; Peponnet, C. Macro to microfluidics system for biological environmental monitoring. *Biosens. Bioelectron.* **2012**, *36*, 230–235.
- (13) Vasudev, A.; Kaushik, A.; Jones, K.; Bhansali, S. Prospects of low temperature co-fired ceramic (LTCC) based microfluidic systems for point-of-care biosensing and environmental sensing. *Microfluid. Nanofluid.* **2013**, *14*, 683–702.
- (14) Jokerst, J. C.; Emory, J. M.; Henry, C. S. Advances in microfluidics for environmental analysis. *Analyst* **2012**, *137*, 24–34.
- (15) Bardin, D.; Kendall, M. R.; Dayton, P. A.; Lee, A. P. Parallel generation of uniform fine droplets at hundreds of kilohertz in a flow-focusing module. *Biomicrofluidics* **2013**, *7*, 34112.
- (16) Choi, K.; Ng, A. H. C.; Fobel, R.; Wheeler, A. R. Digital Microfluidics. In *Annual Review of Analytical Chemistry*; Cooks, R. G., Yeung, E. S., Eds.; Annual Reviews: Palo Alto, CA, 2012; Vol. 5, pp 413–440.
- (17) Fair, R. Digital microfluidics: is a true lab-on-a-chip possible? *Microfluid. Nanofluid.* **2007**, *3*, 245–281.
- (18) Fouillet, Y.; Jary, D.; Chabrol, C.; Claustre, P.; Peponnet, C. Digital microfluidic design and optimization of classic and new fluidic functions for lab on a chip systems. *Microfluid. Nanofluid.* **2008**, *4*, 159–165.
- (19) Abdelgawad, M.; Watson, M. W. L.; Wheeler, A. R. Hybrid microfluidics: A digital-to-channel interface for in-line sample processing and chemical separations. *Lab Chip* **2009**, *9*, 1046–1051.
- (20) Watson, M. W. L.; Jebrail, M. J.; Wheeler, A. R. Multilayer Hybrid Microfluidics: A Digital-to-Channel Interface for Sample Processing and Separations. *Anal. Chem.* **2010**, *82*, 6680–6686.
- (21) Banerjee, A.; Kreit, E.; Liu, Y.; Heikenfeld, J.; Papautsky, I. Reconfigurable virtual electrowetting channels. *Lab Chip* **2012**, *12*, 758–764.
- (22) Dhindsa, M.; Heikenfeld, J.; Kwon, S.; Park, J.; Rack, P. D.; Papautsky, I. Virtual electrowetting channels: electronic liquid transport with continuous channel functionality. *Lab Chip* **2010**, *10*, 832–836.
- (23) Kreit, E.; Mognetti, B. M.; Yeomans, J. M.; Heikenfeld, J. Partial-post laplace barriers for virtual confinement, stable displacement, and >5 cm s^{−1} electrowetting transport. *Lab Chip* **2011**, *11*, 4221–4227.
- (24) Kreit, E.; Dhindsa, M.; Yang, S.; Hagedorn, M.; Zhou, K.; Papautsky, I.; Heikenfeld, J. Laplace Barriers for Electrowetting Thresholding and Virtual Fluid Confinement. *Langmuir* **2010**, *26*, 18550–18556.
- (25) Mugele, F.; Baret, J.-C. Electrowetting: from basics to applications. *J. Phys.: Condens. Matter* **2005**, *17*, R705.
- (26) Berry, S.; Fedynyshyn, T.; Parameswaran, L.; Cabral, A. Reversible Electrowetting on Dual-Scale-Patterned Corrugated Microstructured Surfaces. *J. Microelectromech. Syst.* **2012**, *21*, 1261–1271.
- (27) Chevalliot, S.; Heikenfeld, J.; Clapp, L.; Milarcik, A.; Vilner, S. Analysis of Nonaqueous Electrowetting Fluids for Displays. *J. Display Technol.* **2011**, *7*, 649–656.
- (28) Chatterjee, D.; Hetayothin, B.; Wheeler, A. R.; King, D. J.; Garrell, R. L. Droplet-based microfluidics with nonaqueous solvents and solutions. *Lab Chip* **2006**, *6*, 199–206.
- (29) Yoon, J.-Y.; Garrell, R. L. Preventing Biomolecular Adsorption in Electrowetting-Based Biofluidic Chips. *Anal. Chem.* **2003**, *75*, 5097–5102.
- (30) Pollack, M. G.; Shenderov, A. D.; Fair, R. B. Electrowetting-based actuation of droplets for integrated microfluidics. *Lab Chip* **2002**, *2*, 96–101.
- (31) Bavière, R.; Boutet, J.; Fouillet, Y. Dynamics of droplet transport induced by electrowetting actuation. *Microfluid. Nanofluid.* **2008**, *4*, 287–294.
- (32) Walker, S. W.; Shapiro, B. Modeling the fluid dynamics of electrowetting on dielectric (EWOD). *J. Microelectromech. Syst.* **2006**, *15*, 986–1000.
- (33) Sung Kwon, C.; Shih-Kang, F.; Hyejin, M.; Chang-Jin, K. Towards Digital Microfluidic Circuits: Creating, Transporting, Cutting and Merging Liquid Droplets by Electrowetting-Based Actuation. *The Fifteenth IEEE International Conference on Micro Electro Mechanical Systems*; 2002; pp 32–35.
- (34) Bhattacharjee, B.; Najjaran, H. Droplet sensing by measuring the capacitance between coplanar electrodes in a digital microfluidic system. *Lab Chip* **2012**, *12*, 4416–4423.
- (35) Shih, S. C. C.; Fobel, R.; Kumar, P.; Wheeler, A. R. A feedback control system for high-fidelity digital microfluidics. *Lab Chip* **2011**, *11*, 535–540.
- (36) Sadeghi, S.; Ding, H.; Shah, G. J.; Chen, S.; Keng, P. Y.; Kim, C.-J. C.; van Dam, R. M. On Chip Droplet Characterization: A Practical, High-Sensitivity Measurement of Droplet Impedance in Digital Microfluidics. *Anal. Chem.* **2012**, *84*, 1915–1923.
- (37) Lin, L.; Royal, M. W.; Evans, R.; Fair, R. B.; Jokerst, N. M. Chip Scale Optical Microresonator Sensors Integrated With Embedded Thin Film Photodetectors on Electrowetting Digital Microfluidics Platforms. *IEEE Sens. J.* **2012**, *12*, 1794–1800.
- (38) Zeng, X.; Zhang, K.; Pan, J.; Chen, G.; Liu, A.-Q.; Fan, S.-K.; Zhou, J. Chemiluminescence detector based on a single planar transparent digital microfluidic device. *Lab Chip* **2013**, *13*, 2714–2720.
- (39) Royal, M. W.; Fair, R. B.; Jokerst, N. M. Integrated Sample Preparation and Sensing: Microresonator Optical Sensors Embedded in Digital Electrowetting Microfluidics Systems. *Sensors*; IEEE, 28–31 Oct 2011; pp 2050–2053.
- (40) Banerjee, A.; Liu, Y.; Heikenfeld, J.; Papautsky, I. Deterministic splitting of fluid volumes in electrowetting microfluidics. *Lab Chip* **2012**, *12*, 5138–5141.
- (41) Ren, H. Automated on-chip droplet dispensing with volume control by electro-wetting actuation and capacitance metering. *Sens. Actuators, B* **2004**, *98*, 319–327.
- (42) Gong, J.; Kim, C. C. J. All-electronic droplet generation on-chip with real-time feedback control for EWOD digital microfluidics. *Lab Chip* **2008**, *8*, 898–906.
- (43) Hoshino, T.; Inagaki, F. Molecular quantification of environmental DNA using microfluidics and digital PCR. *Syst. Appl. Microbiol.* **2012**, *35*, 390–395.
- (44) Miller, E. M.; Ng, A. H.; Uddayasankar, U.; Wheeler, A. R. A digital microfluidic approach to heterogeneous immunoassays. *Anal. Bioanal. Chem.* **2011**, *399*, 337–345.
- (45) Ng, A. H.; Uddayasankar, U.; Wheeler, A. R. Immunoassays in microfluidic systems. *Anal. Bioanal. Chem.* **2010**, *397*, 991–1007.
- (46) Jebrail, M. J.; Luk, V. N.; Shih, S. C. C.; Fobel, R.; Ng, A. H. C.; Yang, H.; Freire, S. L. S.; Wheeler, A. R. Digital Microfluidics for Automated Proteomic Processing. *J. Vis. Exp.* **2009**, e1603.
- (47) Bogojevic, D.; Chamberlain, M. D.; Barbulovic-Nad, I.; Wheeler, A. R. A digital microfluidic method for multiplexed cell-based apoptosis assays. *Lab Chip* **2012**, *12*, 627–634.
- (48) Noh, J. H.; Noh, J.; Kreit, E.; Heikenfeld, J.; Rack, P. D. Toward active-matrix lab-on-a-chip: programmable electrofluidic control enabled by arrayed oxide thin film transistors. *Lab Chip* **2012**, *12*, 353–360.